ORGANIC CHEMISTRY FRONTIERS

RESEARCH ARTICLE

View Article Online
View Journal | View Issue

Cite this: *Org. Chem. Front.*, 2025, **12**, 1763

Synthesis and chiral self-sorting of spirobifluorene-containing boronate ester cages†‡

Natalie Schäfer,[a,b] Lukas Glanz,[c] Arne Lützen [c] and Florian Beuerle [*a,b,d]

2,2′-Functionalization induces axial chirality within the orthogonal aromatic scaffold of 9,9′-bispirofluorene. By implementing boronic acids at these positions, well-suited precursors for chiral boronate ester cages are generated. As a key intermediate, (*P*)-9,9′-bispirofluorene-2,2′-bistriflate (*P*)-**5** was synthesized *via* a four-step sequence of twofold Friedel–Crafts acylation, Baeyer–Villiger oxidation, hydrolysis, and triflate formation. Chiral resolution was achieved *via* chiral HPLC for the dihydroxy intermediate. In a modular manner, Pd-catalyzed borylation or cross-coupling afforded either diboronic acid (*P*)-**B*** or elongated derivative (*P*)-**B*^{Ph}** possessing additional phenylene spacers. For both enantiomerically pure linkers, reaction with hexahydroxy tribenzotriquinacene **A** in THF under water-removing conditions afforded isoreticular chiral organic cages (*P*,*P*,*P*)-**$A_2B^*_3$** and (*P*,*P*,*P*)-**$A_2B^{*Ph}_3$**. Both cages possess a chiral trigonal–bipyramidal geometry and were characterized by ^{1}H, ^{13}C and DOSY NMR spectroscopy and MALDI-TOF mass spectrometry. Chiral self-sorting of the bispirofluorene precursors was investigated by reactions of **A** with racemic linkers *rac*-**B*** and *rac*-**B*^{Ph}**. For shorter linker *rac*-**B***, quantitative self-sorting into a racemic mixture of (*P*,*P*,*P*)-**$A_2B^*_3$** and (*M*,*M*,*M*)-**$A_2B^*_3$** occurred. For elongated derivative *rac*-**B*^{Ph}** however, the increased flexibility introduced by the phenylene extension resulted in much lower selectivity and self-recognition. Instead a more complex product mixture was obtained and the racemic mixture of **$A_2B^{*Ph}_3$** was isolated in much lower yield of around 20%. Semiempirical PM6 calculations for both homo- and heterochiral cages and macrocyclic intermediates allowed for an estimation of macrocyclic strain energies and provided in-depth insight into cage formation pathways and self-sorting properties.

Received 25th October 2024,
Accepted 21st January 2025

DOI: 10.1039/d4qo02012j

rsc.li/frontiers-organic

Introduction

Chirality is omnipresent in nature, arts and science. Down to the molecular level, humans have always been fascinated and inspired by objects that do not superpose with their mirror image. But besides structural aesthetics, impressive function is also demonstrated through the unrivalled selectivity and efficiency of enzymes and biological receptors. To mimic the well-defined cavities of natural catalysts or hosts, chiral covalent organic cages[1–5] are intriguing model compounds.[6,7] However, the typical synthesis through dynamic covalent reactions between small organic building blocks favours highly symmetrical topologies,[8] which makes the formation of intrinsically chiral and asymmetric cavities still a challenging task. In principle, three different strategies are conceivable for the synthesis of chiral cages: (i) The implementation of different precursors at spatially specified positions, *e.g.*, four different subunits at the corners of a tetrahedral cage, (ii) the implementation of chiral precursors as vertices[9–12] or edges[13–15] in otherwise achiral cage geometries, or (iii) the attachment of chiral substituents.[16] While the first approach would require highly sophisticated self-sorting or large chiral templates, and has therefore not been realized until now, an intriguing example for the formation of topologically chiral cage catenanes based on achiral monomers was recently reported by Zhang and coworkers.[17] Otherwise, several examples for cage synthesis with chiral starting materials have been reported. These cages were applied in asymmetric Michael additions[14] or aldol reactions,[16] enantioselective separation,[7,13,18] chiroptical amplification,[15] or the formation of chiral frameworks *via* cage-to-COF transformation with a chiral memory effect.[19]

Due to the rigid modular assembly, the chirality of the individual chiral building blocks might be amplified within the

[a]*Julius-Maximilians-Universität Würzburg, Institut für Organische Chemie, Am Hubland, 97074 Würzburg, Germany*
[b]*Julius-Maximilians-Universität Würzburg, Center for Nanosystems Chemistry (CNC), Theodor-Boveri-Weg, 97074 Würzburg, Germany*
[c]*Universität Bonn, Kekulé-Institut für Organische Chemie und Biochemie, Gerhard-Domagk-Straße 1, 53121 Bonn, Germany*
[d]*Eberhard Karls Universität Tübingen, Institut für Organische Chemie, Auf der Morgenstelle 18, 72076 Tübingen, Germany.*
E-mail: florian.beuerle@uni-tuebingen.de

† Dedicated to Prof. Dr. Frank Würthner on the occasion of his 60th birthday.

‡ Electronic supplementary information (ESI) available: Synthetic procedures and characterization, DOSY data, self-sorting experiments, molecular modelling. See DOI: https://doi.org/10.1039/d4qo02012j

well-defined 3D cage assembly, and even new properties and effects could emerge *via* the mutual interaction between these subunits. While synthesis from enantiopure starting materials will always end up in homochiral assemblies, racemic precursors might lead to more complex reactions, which could also give diastereomeric assemblies and chiral self-sorting might occur.[20] Such recognition processes have presumably played a significant role during the evolution of homochiral biological systems, which makes investigations towards self-sorting in organic cages very interesting model studies. In a landmark example, the Mastalerz group studied the self-sorting in tribenzotriquinacene-based (TBTQ) imine cages with either $[2 + 3]^9$ or cubic $[8 + 12]^{10}$ stoichiometry.

Here we report on the synthesis and characterization of two isoreticular chiral [2 + 3] boronate ester cages based on tripodal TBTQ nodes and chiral spirobifluorene (SBF) linkers. While homochiral [2 + 3] assemblies are obtained from enantiomerically enriched linkers, self-sorting was investigated for the synthesis with racemic precursors.

Results and discussion

Boronate ester condensations are well-established dynamic covalent reactions that have been frequently used for the synthesis of macrocycles[21–23] and cages.[24–30] In previous work, we synthesized a series of shape persistent trigonal bipyramidal A_2B_3, tetrahedral A_4C_6 and cubic A_8D_{12} cages *via* multiple boronate ester formation between hexahydroxy tribenzotriquinacenes (TBTQ) and diboronic acids with varying bite angle.[31–33] Depending on the steric demand of the apical substituent R at the TBTQ vertices, either soluble cages[34] (R = ^{n}Bu) or crystalline cage materials (R = Me) with excellent porosity[35] can be obtained. Upon steric shielding of the labile boronate esters, cubic cages with unprecedented hydrolytic stability were synthesized.[36] For all these structures, the highly directional and linear dioxaborolane linkages induce the formation of highly symmetrical and achiral cage geometries. As the most obvious point to introduce chirality into such highly symmetrical cage geometries, we identified the bent diboronic acid linkers.

Molecular design

As potential building blocks for chiral A_2B_3 cages, suitably substituted 9,9′-spirobifluorenes[37] (SBFs) seemed very promising as these have proven their versatility as a rigid V-shaped scaffold in a broad variety of applications ranging from molecular recognition[38–42] and sensing,[43] to metallosupramolecular chemistry[44–46] and even catalysis[47–49] and opto-electronic materials.[37,50–52] Hence, we envisioned the use of two diboronic acid linkers **B*** and **B*^{Ph}**, based on the intrinsically chiral 2,2′-difunctionalized SBF scaffold also for our purposes. While in **B*** the boronic acid sites are directly attached in 2,2′-position, additional phenylene spacers are introduced in **B*^{Ph}**. This spatial elongation creates an isoreticular cage with similar geometry but extended edges and, thus, an enlarged cavity. On the other hand, the additional phenylene units add structural flexibility, which might influence the assembly pathway and selectivity for the targeted cage. Owing to the orthogonal spiro-connection of the fluorene units, the two boronic acid moieties span a bite angle of roughly 90°, which is close enough to the preferred angle of 70.5° for a strain-free [2 + 3] cage[31] to expect successful cage formation.

Synthesis of chiral linkers

The synthesis of diboronic acids **B*** and **B*^{Phe}** (Scheme 1) largely builds on known SBF derivatives which have been reported by us and others.[53–56] Twofold Friedel–Crafts acylation of parent spirobifluorene (**1**)[56] in 2,2′-positions followed by Baeyer–Villiger oxidation and saponification with NaOH gave racemic diol **4**[54] as key intermediate in 67% yield over three steps (for more details on synthetic procedures and analytical data see ESI‡). At this stage, the enantiomers could be separated by chiral HPLC.[53] Both the racemate and the pure *P* isomer were converted to the bistriflates *rac*-**5** and (*P*)-**5**,[55] respectively, which served as precursors for the direct implementation of the boronic acid sites or an isoreticular phenylene extension.

On the one hand, Pd-catalysed borylation with bis(pinacolato)-diboron[55] and subsequent deprotection under acidic conditions afforded the shorter chiral linkers *rac*-**B*** and (*P*)-**B***. On the other hand, Suzuki–Miayura reaction with 4-(trimethylsilyl)-phenylboronic acid (**6**) followed by direct transformation of the silyl groups into boronic acids with BBr_3 yielded the elongated linkers *rac*-**B*^{Phe}** and (*P*)-**B*^{Phe}**.

Synthesis of chiral cages

With this series of chiral SBF units at hand, cage synthesis was performed under previously established conditions.[31,32]

Initially, we investigated reactions between hexahydroxy TBTQ **A** and enantiomerically pure SBF derivatives. For the shorter linker, **A** and (*P*)-**B*** were dissolved in THF-d_8 in 2 : 3 molar ratio and, subsequently, 4 Å molecular sieves were added. ^{1}H NMR reaction monitoring of the bridgehead methine protons showed a quantitative downfield shift towards one singlet at δ = 4.43 ppm after five days, thus indicating the formation of a highly symmetrical structure (Fig. 1a). Intriguingly, only very small amounts of doubly condensed TBTQ species were identified during the reaction (Fig. 1b), suggesting a smooth cage formation and cooperative closure of the final binding site. After removal of the solvent, pure cage **$A_2B^*_3$** was isolated in 74% yield and the obtained solid was easily dissolved in $CDCl_3$ for further characterization. In contrast to previously reported **A_2B_3** cages based on *ortho*-terphenyl linkers with point group D_{3h}, symmetry is reduced to D_3 after implementation of chiral SBF units, which is, *e.g.*, illustrated by the splitting of the aromatic TBTQ protons into two singlets at δ = 7.19 and 7.12 ppm (Fig. 1a). MALDI-TOF MS measurements (Fig. 1c) only revealed the molecular ion peak for **$A_2B^*_3$** at *m*/*z* = 1860.2474 and no signals for any smaller or larger assemblies. From DOSY NMR measurements in $CDCl_3$ (Fig. 1d), a diffusion constant of $D = 3.84 \times 10^{-10}$ m^2 s^{-1} was obtained.

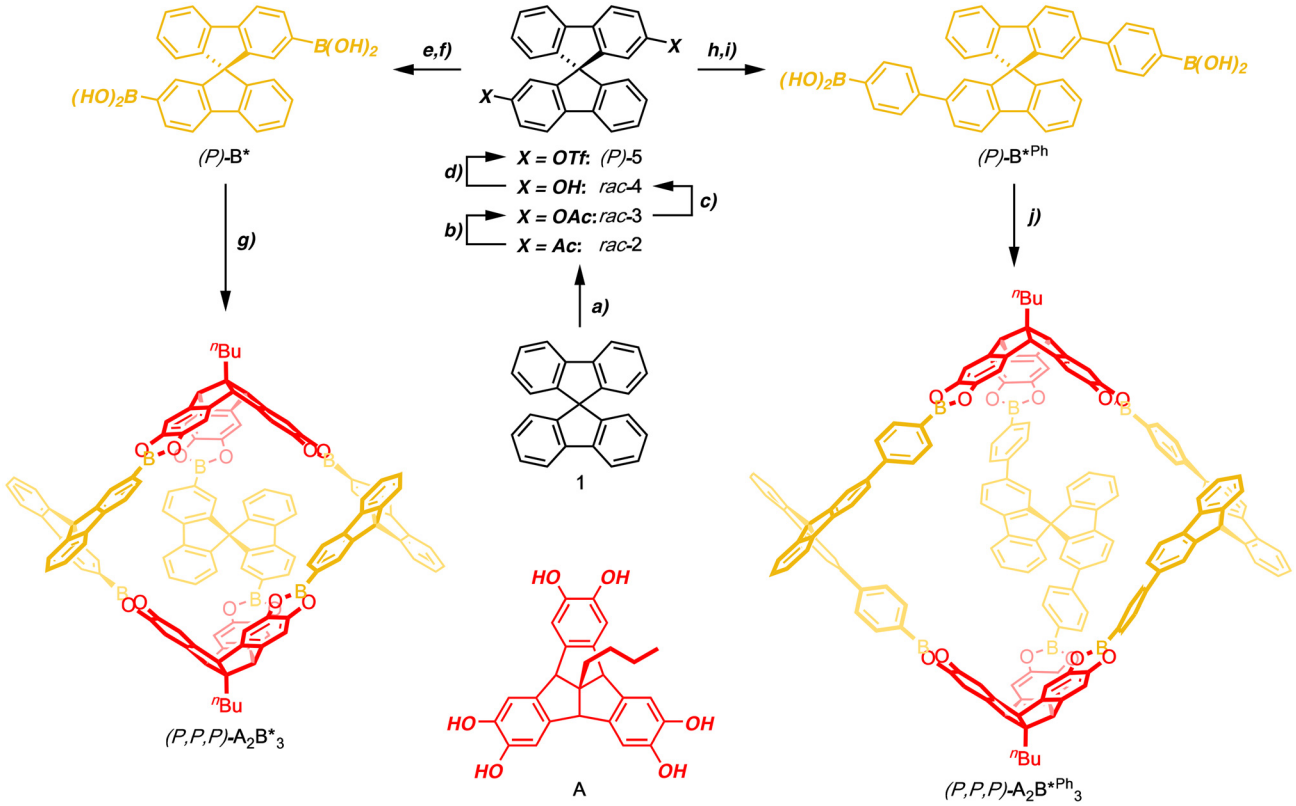

Scheme 1 Synthesis of chiral linkers and cages: (a) $AlCl_3$/AcCl, CH_2Cl_2/$MeNO_2$ 1 : 1, rt, 12 h, 96%;[53] (b) *m*CPBA, CH_2Cl_2, 45 °C, 2 d, 73%;[54,55] (c) NaOH/H_2O, MeOH, 50 °C, 10 min, 96%;[54] (d) 1. HPLC separation,[53] 2. Tf_2O/NEt_3, CH_2Cl_2, −78 °C, 2 h, 73%;[55] (e) $Pd(OAc)_2$/XPhos/KOAc/B_2pin_2, 1,4-dioxane, 110 °C, 1 d, 99%,[55] (f) $MeB(OH)_2$/TFA, CH_2Cl_2, rt, 1 d, (*P*): 72%, *rac*: 68%; (g) **A**, 4 Å MS, THF, rt, 5 d, 74%; (h) $Pd(OAc)_2$/SPhos/K_3PO_4/4-TMSPhB$(OH)_2$, 1,4-dioxane/H_2O 5 : 1, 100 °C, 1 d, 93%; (i) BBr_3, CH_2Cl_2, rt, 2 h, (*P*): 98%, *rac*: 67%; (j) **A**, 4 Å MS, THF, rt, 14 d, 65%.

The solvodynamic radius of r_{solv} = 1.01 nm calculated according to the Stokes–Einstein equation[34] is in good agreement with a PM6-optimized[57] molecular model of the intended $\mathbf{A_2B^*_3}$ cage (transparent sphere in Fig. 1d).

Under the same conditions, TBTQ **A** and elongated linker (*P*)-$\mathbf{B^{*Ph}}$ were dissolved in THF-d_8 in 2 : 3 molar ratio and 4 Å molecular sieves were added. In contrast to the smooth formation of $\mathbf{A_2B^*_3}$, reaction monitoring by ^{1}H NMR spectroscopy indicated a much slower and imperfect cage formation. Even after eight days, no quantitative conversion was achieved, and minor impurities are still observable besides the main product (Fig. 2a, b and S26‡). As another difference to the smaller linker, free **A** is quickly consumed but twofold condensation products of **A** are dominant species during the reaction (Fig. 2b). After evaporating the solvent, the main species was separated from the impurities and isolated in 65% yield by dissolving in $C_2D_2Cl_4$ (Fig. S25‡). Again, D_3 symmetry of the isolated $\mathbf{A_2B^{*Ph}_3}$ is evidenced by one singlet of the methine protons at δ = 4.56 ppm and a splitting of the aromatic TBTQ protons at δ = 7.40 and 7.38 ppm. MALDI-TOF MS measurements of isolated $\mathbf{A_2B^{*Ph}_3}$ (Fig. 2c) only showed the molecular ion peak at m/z = 2317.0865. Finally, DOSY NMR measurements in $C_2D_2Cl_4$ (Fig. 2d) revealed a diffusion coefficient of D = 1.02 × 10^{-10} m^2 s^{-1} and a solvodynamic radius of r_{solv} = 1.25 nm,[34] which resembles well to the elongated spacing between the two opposing TBTQ units. Overall, the combined analytical data strongly supports the formation of chiral cage (*P*,*P*,*P*)-$\mathbf{A_2B^{*Ph}_3}$ as the main species.

Self-sorting experiments

To elaborate on the self-sorting properties of these chiral SBF linkers, cage reactions were repeated with racemic mixtures of the diboronic acids under otherwise identical conditions. In case of narcissistic self-sorting, the respective enantiomers of the chiral linkers would recognize and select likewise molecules to form a racemic mixture of homochiral [2 + 3] cages with either (*P*,*P*,*P*) or (*M*,*M*,*M*) configuration. On the other hand, preference for mixed assemblies might either lead to social self-sorting into well-defined heterochiral assemblies or the unselective formation of ill-defined oligomeric products.

For *rac*-**B***, similar observations as for (*P*)-**B*** by ^{1}H NMR spectroscopy indicated quantitative cage formation after five days. During the reaction, the TBTQ methine protons again showed only a small fraction of doubly condensed TBTQ species, and just one sharp singlet at the end of the reaction (Fig. 3a). After workup, *rac*-$\mathbf{A_2B^*_3}$ was isolated in astonishingly 94% yield, which was even higher as for the enantiopure cage. As ^{1}H NMR spectroscopy for the reaction mixtures after five

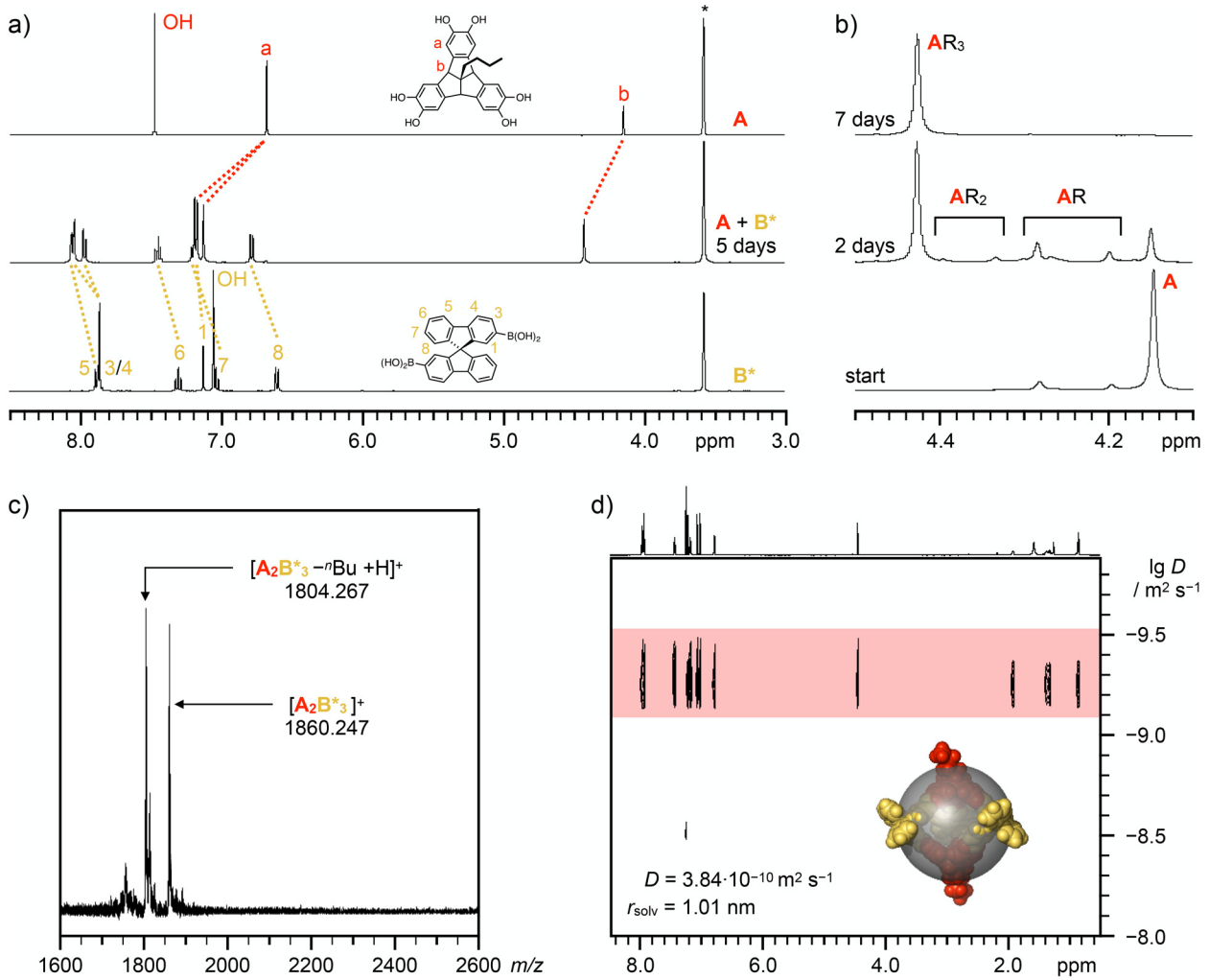

Fig. 1 (a) Partial ^{1}H NMR spectra (400 MHz, THF-d_8, 295.6 K) of TBTQ **A** (top), the finished reaction mixture of **A** and (*P*)-**B*** after five days (middle) and (*P*)-**B***; (b) ^{1}H NMR reaction monitoring for the bridgehead methine protons directly after mixing (bottom) and after two (middle) and seven (top) days indicating the increasing degree of boronate ester formation in **A**; (c) MALDI-TOF MS and (d) DOSY NMR spectrum (400 MHz, $CDCl_3$, 295.6 K) of (*P,P,P*)-**A$_2$B*$_3$** (PM6-minimized[57] space-filling model with the solvodynamic radius indicated as a semi-transparent grey sphere, image created with PyMOL[58]).

days indicated quantitative cage formation in both cases, we attribute the lower isolated yield for the homochiral cage to a lower solubility and a more difficult resolvation. As both isolated (*P*)-**A$_2$B*$_3$** and *rac*-**A$_2$B*$_3$** revealed identical ^{1}H (Fig. S37 and S38‡), ^{13}C (Fig. S39‡) and DOSY NMR ($D = 3.79 \times 10^{-10}$ m^2 s^{-1}, r_{solv} = 1.02 nm for *rac*-**A$_2$B*$_3$**, Fig. S33 and S34‡) data as well as MALDI-TOF mass spectra (Fig. S40‡), exclusive narcissistic self-sorting into enantiomeric cages (*P,P,P*)-**A$_2$B*$_3$** and (*M,M,M*)-**A$_2$B*$_3$** is evident for the reaction between **A** and *rac*-**B***.

For elongated **B*^{Ph}** however, a more complex picture emerged. Initially after the addition of 4 Å molecular sieves, boronate ester formation proceeded quickly with fast consumption of **A** and its monoester. MALDI-TOF MS after six days (Fig. S43‡) revealed a complex mixture consisting of boronate ester assemblies with [2 + 2], [2 + 3] and [2 + 4] **A : B*^{Ph}** stoichiometry alongside **(B*^{Ph})$_3$** boroxine species with [0 + 3], [1 + 3] and [1 + 4] stoichiometry (see Fig. S44‡ for proposed molecular structures). After about a week though, precipitation started and continued for another week. By comparison with data for (*P,P,P*)-**A$_2$B*$^{Ph}_3$**, the remaining solution contained *rac*-**A$_2$B*$^{Ph}_3$** as one plausible component besides larger amounts of byproducts (Fig. 3b and S42‡). The isolated precipitate was not soluble in $CDCl_3$ even at elevated temperature. However, a soluble fraction was obtained in around 25% yield after stirring over anhydrous $C_2D_2Cl_4$ at 130 °C. After careful removal of the solvent, ^{1}H NMR spectroscopy after resolvation in $CDCl_3$ revealed a mixture of two main species (Fig. S45‡). Due to the excellent agreement with data for (*P,P,P*)-**A$_2$B*$^{Phe}_3$**, the major component is identified as the racemic mixture of (*P,P,P*) and (*M,M,M*) cages. For the minor component, NMR integration indicated a 1 : 1 ratio for precursors **A** and **B*^{Phe}**. In contrast to D_3 symmetrical A_2B_3 cages, the side product exhibited reduced symmetry. For instance, both methine and aromatic protons of

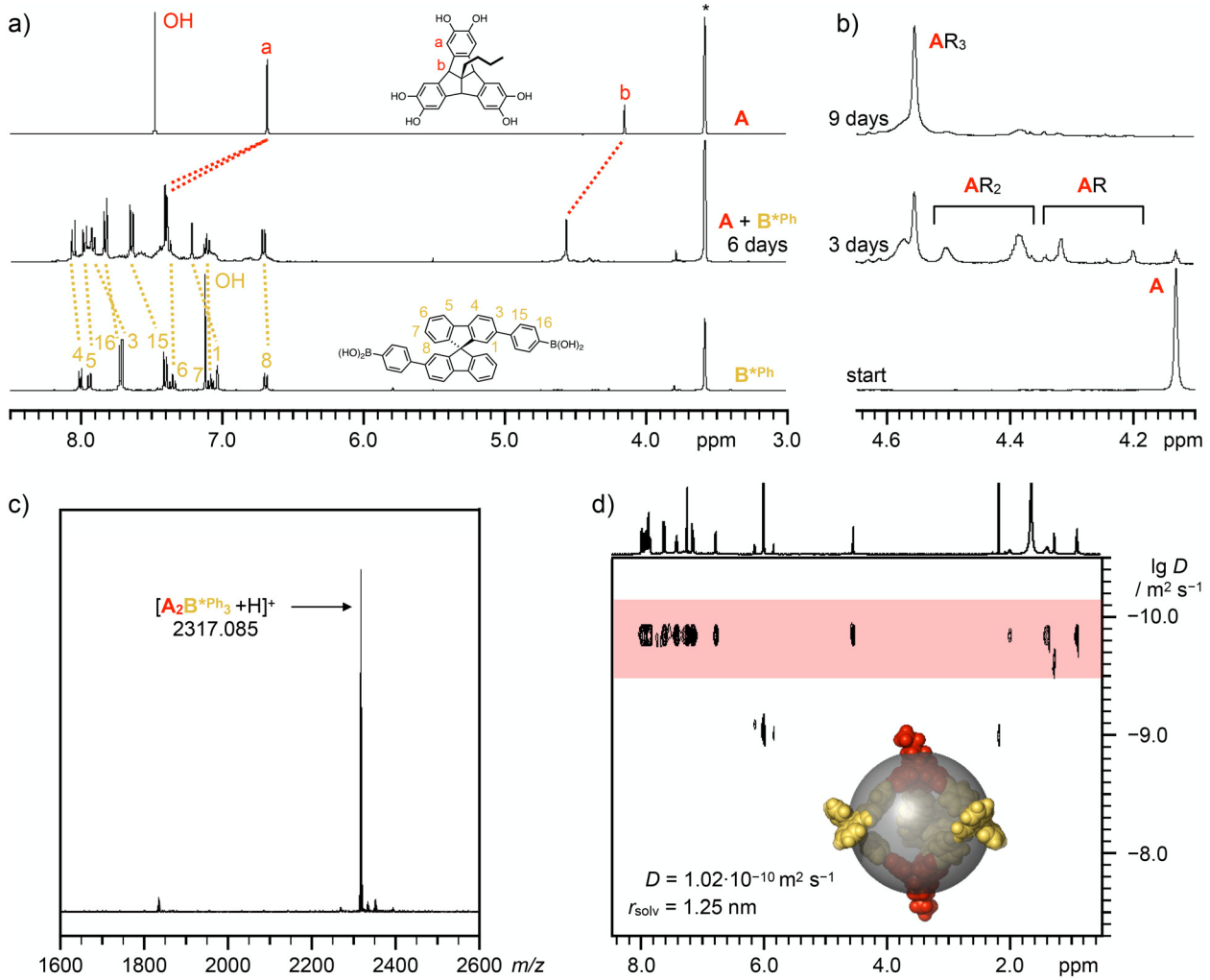

Fig. 2 (a) Partial ^{1}H NMR spectra (400 MHz, THF-d_8, 295.6 K) of TBTQ **A** (top), the reaction mixture of **A** and (*P*)-**B*^{Ph}** after six days (middle) and chiral (*P*)-**B*^{Ph}** (bottom); (b) ^{1}H NMR reaction monitoring for the bridgehead methine protons directly after mixing (bottom) and after three (middle) and nine (top) days indicating the increasing degree of boronate ester formation in **A**; (c) MALDI-TOF MS and (d) DOSY NMR spectrum (400 MHz, $C_2D_2Cl_4$, 295.6 K) of (*P,P,P*)-**A$_2$B*$^{Ph}_3$** (PM6-minimized[57] space-filling model with the solvodynamic radius indicated as a semi-transparent grey sphere, image created with PyMOL[58]).

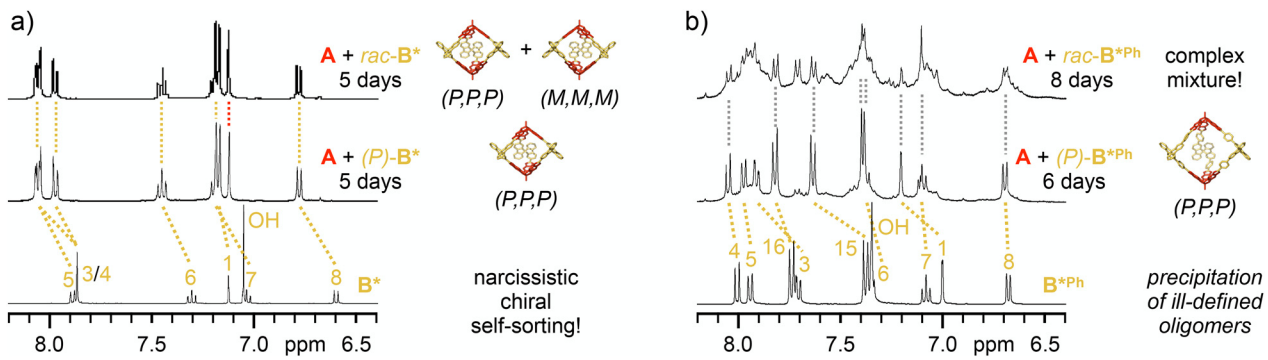

Fig. 3 ^{1}H NMR reaction monitoring (400 MHz, THF-d_8, 298 K) for (a) narcissistic chiral self-sorting (top) into racemic cages *rac*-**A$_2$B*$_3$** for the reaction of diboronic acid *rac*-**B*** with TBTQ **A** (top, homochiral cages (*P,P,P*)-**A$_2$B*$_3$** (middle) and free linker **B*** (bottom) as references) and (b) self-sorting experiment (top) for the reaction of diboronic acid *rac*-**B*^{Ph}** with TBTQ **A** (homochiral cages (*P,P,P*)-**A$_2$B*$^{Ph}_3$** (middle) and free linker **B*^{Ph}** (bottom) as references).

the TBTQ units split into three and six singlets, respectively, and two sets of doublets were observed for the phenylene extensions of the linkers (Fig. S47‡). MALDI-TOF mass spectra revealed the molecular ion peak for *racemic* $\mathbf{A_2B^{*Phe}_3}$ at m/z = 2317.0768 and a smaller signal at m/z = 1832.7957 corresponding to a macrocyclic $\mathbf{A_2B^{*Phe}_2}$ intermediate (Fig. S48‡). Unfortunately, DOSY NMR data for this mixture of at least two components could not be fitted with a biexponential decay, but nevertheless hint towards [2 + 3] and [2 + 2] assemblies without evidence of larger structures (Fig. S35 and S36‡). Based on these combined data, the major and minor species can presumably be assigned to *racemic* $\mathbf{A_2B^{*Phe}_3}$ and a racemic mixture of a homochiral $\mathbf{A_2B^{*Phe}_2}$ macrocyclic intermediate, respectively. Based on NMR integration, these compounds are present in 3 : 1 ratio and are isolated in a combined yield of roughly 25%.

Molecular modeling

For further insight into self-sorting properties and relative stabilities for the various homo- and heterochiral assemblies, we performed quantum-chemical calculations. To estimate any strain energy that is accumulated during ring-closing reactions towards macrocyclic intermediates and the ultimate cages, we defined a series of homodesmotic reactions which assemble these structures from the respective building blocks (see Section 6 in the ESI for more details‡). Thereby, we assume that any solvent effects or enthalpic contributions of the boronate ester formations are cancelled out and, in first approximation, only the macrocyclic strain is recognized. This strain energy for a given structure is calculated as the reaction enthalpy for its homodesmotic formation calculated from the heats of formation obtained after semiempirical PM6 geometry optimizations in the gas phase with Spartan'20 [57] for all involved structures (Fig. S49 and Table S2‡). Since both building blocks possess rather rigid bite angles very close to 90°, we only considered [2 + 2] macrocyclic and [2 + 3] cage assemblies as any larger structures are unfeasible due to severe strain and have not been observed experimentally by MALDI TOF MS. For the macrocycles, two homochiral configurations with either *cis*- or *trans*-arrangement of the two unreacted catechol sites and three heterochiral assemblies (1× *cis* and 2× *trans*) are conceivable. In addition, the two diastereomeric cages with either (*P*,*P*,*P*) or (*P*,*P*,*M*) configuration have been calculated. For the mechanism of cage formation, it must be noted that only the *cis*-macrocycles may be further converted into cages, whereas the *trans*-isomers are *off-pathway* intermediates towards oligomeric side products.

Looking on these data, some remarkable differences between the two linkers become evident (Fig. 4).

For **B***, the direct attachment of the boronic acid groups to the SBF core significantly rigidifies any boronate ester assemblies. Despite the pairwise matching 90° bite angles, the twisted orientation of the aromatic wings in **A** and **B*** prevents the strain-free formation of square-shaped [2 + 2] macrocycles. The most stable isomer has *cis*-(*P*,*P*) configuration for which the two unreacted catechols are tilted towards each other to maximize π overlap between the dioxaborolane and adjacent phenyl rings with an inherent strain energy of 5.5 kJ mol^{-1} compared to the free precursors. Intriguingly, this *on-pathway* intermediate is perfectly predisposed and preorganized for the addition of a third linker (*P*)-**B*** toward homochiral (*P*,*P*,*P*)-$\mathbf{A_2B^*_3}$, which is best illustrated by the nearly perfect overlay for PM6-optimized structures of *cis*-(*P*,*P*)-$\mathbf{A_2B^*_3}$ and (*P*,*P*,*P*)-$\mathbf{A_2B^*_3}$ (Fig. S50‡). No reorganization is needed for the final ring closure, which does not add significant strain energy towards the closed homochiral cage assembly (Fig. 4). In contrast to this convergent pathway, all other macrocyclic intermediates are significantly higher in energy and also the heterochiral

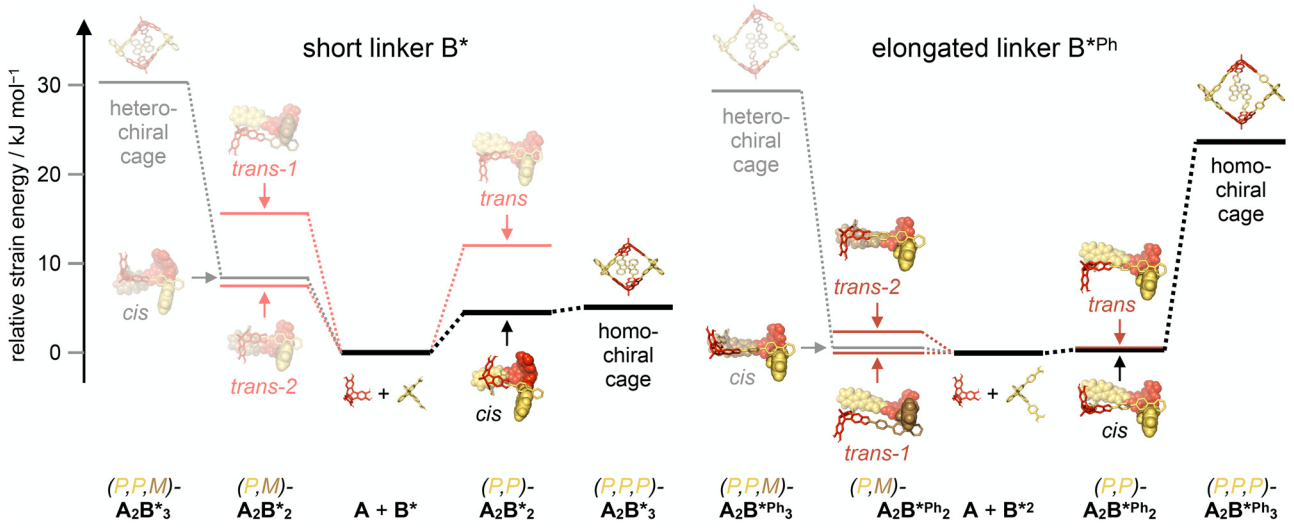

Fig. 4 Relative strain energies (kJ mol^{-1}; obtained from reaction enthalpies for homodesmotic reactions calculated from heats of formation from semiempirical PM6 geometry optimization with Spartan'20[57]) of homo- and heterochiral macrocyclic A_2B_2 intermediates and A_2B_3 cages for reactions between TBTQ **A** and chiral SBF linkers **B*** (left) and **B*^{Ph}** (right); images of the optimized structures were created with PyMol.[58]

cage is thermodynamically disfavoured. These calculations are in line with experimental observations, as we observed facile and emergent formation of homochiral cages even for *rac*-**B***. In an "*all or nothing*" fashion, most of the strain energy is already built up in the first macrocycle, which is cooperatively transformed into the cage with a high effective molarity for the final cyclization. The large energetic separation between homo- and heterochiral product induced strong narcissistic self-sorting for racemic mixtures.

For the elongated $\mathbf{B}^{*Ph}$, the potential hypersurface looks rather different. With the insertion of an additional phenylene unit between the dioxaborolane and the SBF unit, interactions are independent of the relative orientation of the TBTQ and SBF units but can be fine-tuned by rotation of the phenylene spacer. Therefore, all four possible macrocycles are almost strain-free with a square shape and parallel alignment of the free catechols on opposite corners. In contrast to the smaller cage, these reactive sites must be brought together to introduce the missing linker, and the entire strain energy is only accumulated in the final cyclization step (Fig. S50‡). This differing stability is also reflected in the experiments. When monitoring the formation of the larger cage by ^{1}H NMR, fast consumption of **A** and monoester was observed. However, twofold boronate ester assemblies are accumulated for several days. This reflects the formation of macrocylces as rather stable resting states. Only by the slow removal of water, the less favorable equilibrium for the final cyclization is gradually shifted towards completely reacted (*P*,*P*,*P*)-$\mathbf{A_2B^{*Ph}}_3$. But even after two weeks, traces of partially reacted intermediates are still visible in ^{1}H NMR (Fig. 2c). Recently, we made a similar observation of long-lived macrocyclic intermediates during the synthesis of highly strained A_2C_3 cages templated by endohedral hydrogen bonding.[33]

For reaction of (*P*)-$\mathbf{B}^{*Ph}$, the dynamic equilibrium between *cis* and *trans* macrocycle slowly converts most of the precursors into cages, as evident by the isolated yield of 65%. For the self-sorting experiments however, the additional *meso*-macrocycles make the product distribution even more complex and apparently give access to other heterochiral oligomers which precipitate over time. The minor component in the isolated product might be either the *trans* or *cis* macrocyle, which cannot be discriminated by NMR. It is unclear at this point if this side product is already present in the precipitate or if it is only formed during the solvation as the release of strain energy after cage opening might be facilitated in the presence of even traces of water.

Conclusions

Two isoreticular chiral boronate ester cages (*P*,*P*,*P*)-$\mathbf{A_2B^*}_3$ and (*P*,*P*,*P*)-$\mathbf{A_2B^{*Ph}}_3$ were synthesized by condensation of hexahydroxy TBTQ **A** and axially chiral SBF derivatives (*P*)-**B*** or (*P*)-$\mathbf{B}^{*Ph}$, respectively. The isoreticular extension of the trigonal–bipyramidal assemblies was confirmed by ^{1}H DOSY NMR spectroscopy and an increase of the solvodynamic radius from 1.01 to 1.25 nm due to the phenylene extension in $\mathbf{B}^{*Ph}$. Self-sorting experiments with racemic SBF precursors revealed quantitative narcissistic self-sorting behavior for more rigid **B*** into a racemic mixture of (*P*,*P*,*P*)-$\mathbf{A_2B^*}_3$ and (*M*,*M*,*M*)-$\mathbf{A_2B^*}_3$. Evaluation of the inherent strain energies by semiempirical PM6 calculations for homodesmotic cage forming reactions revealed that the thermodynamically preferred homochiral *cis*-$\mathbf{A_2B^*}_2$ macrocycles are highly predisposed and preorganized to accelerate final ring closure and guide cage formation towards the homochiral assemblies. In contrast, the more flexible $\mathbf{B}^{*Ph}$ leads to strain-free $\mathbf{A_2B^{*Ph}}_2$ square macrocycles that serve as resting state and that could be either slowly converted into homochiral cages or form ill-defined heterochiral oligomers as side products in self-sorting reactions.

These shape-persistent cages generate well-defined chiral cavities in the nm range and stereoselective host–guest chemistry is currently investigated. On the other hand, valuable insight into kinetic and thermodynamic aspects of cage formation mechanisms have been provided that enhance fundamental understanding in dynamic covalent chemistry and will guide the design and synthesis of novel tailormade materials based on porous organic cages.

Data availability

The data supporting this article have been included as part of the ESI.‡

Conflicts of interest

There are no conflicts to declare.

Acknowledgements

Financial support by the DFG (BE4808/2-1) is gratefully acknowledged.

References

1 F. Beuerle and B. Gole, Covalent Organic Frameworks and Cage Compounds: Design and Applications of Polymeric and Discrete Organic Scaffolds, *Angew. Chem., Int. Ed.*, 2018, **57**, 4850–4878.
2 G. Zhang and M. Mastalerz, Organic cage compounds – from shape-persistency to function, *Chem. Soc. Rev.*, 2014, **43**, 1934–1947.
3 T. Kunde, T. Pausch and B. M. Schmidt, Porous Organic Compounds – Small Pores on the Rise, *Eur. J. Org. Chem.*, 2021, 5844–5856.
4 G. Montà-González, F. Sancenón, R. Martínez-Máñez and V. Martí-Centelles, Purely Covalent Molecular Cages and Containers for Guest Encapsulation, *Chem. Rev.*, 2022, **122**, 13636–13708.

5 X. Yang, Z. Ullah, J. F. Stoddart and C. T. Yavuz, Porous Organic Cages, *Chem. Rev.*, 2023, **123**, 4602–4634.
6 M. Raynal, P. Ballester, A. Vidal-Ferran and P. W. N. M. van Leeuwen, Supramolecular catalysis. Part 2: artificial enzyme mimics, *Chem. Soc. Rev.*, 2014, **43**, 1734–1787.
7 L. Chen, P. S. Reiss, S. Y. Chong, D. Holden, K. E. Jelfs, T. Hasell, M. A. Little, A. Kewley, M. E. Briggs, A. Stephenson, K. M. Thomas, J. A. Armstrong, J. Bell, J. Busto, R. Noel, J. Liu, D. M. Strachan, P. K. Thallapally and A. I. Cooper, Separation of rare gases and chiral molecules by selective binding in porous organic cages, *Nat. Mater.*, 2014, **13**, 954–960.
8 S. Ivanova and F. Beuerle, Porous Crystalline Organic Cages Made by Design, *Isr. J. Chem.*, 2024, **64**, e202400025.
9 D. Beaudoin, F. Rominger and M. Mastalerz, Chiral Self-Sorting of [2 + 3] Salicylimine Cage Compounds, *Angew. Chem., Int. Ed.*, 2017, **56**, 1244–1248.
10 P. Wagner, F. Rominger, W.-S. Zhang, J. H. Gross, S. M. Elbert, R. R. Schröder and M. Mastalerz, Chiral Self-sorting of Giant Cubic [8 + 12] Salicylimine Cage Compounds, *Angew. Chem., Int. Ed.*, 2021, **60**, 8896–8904.
11 H. Qu, X. Tang, X. Wang, Z. Li, Z. Huang, H. Zhang, Z. Tian and X. Cao, Chiral molecular face-rotating sandwich structures constructed through restricting the phenyl flipping of tetraphenylethylene, *Chem. Sci.*, 2018, **9**, 8814–8818.
12 X. Tang, Z. Li, H. Liu, H. Qu, W. Gao, X. Dong, S. Zhang, X. Wang, A. C.-H. Sue, L. Yang, K. Tan, Z. Tian and X. Cao, Hollow and highly diastereoselective face-rotating polyhedra constructed through rationally engineered facial units, *Chem. Sci.*, 2021, **12**, 11730–11734.
13 M. Mohan, D.-J. Pham, A. Fluck, S. Chapuis, A. Chaumont, B. Kauffmann, L. Barloy and P. Mobian, A Chiral [2 + 3] Covalent Organic Cage Based on 1,1′-Bi-2-naphthol (BINOL) Units, *Chem. – Eur. J.*, 2024, **30**, e202400458.
14 K. Wang, X. Tang, B. A. Anjali, J. Dong, J. Jiang, Y. Liu and Y. Cui, Chiral Covalent Organic Cages: Structural Isomerism and Enantioselective Catalysis, *J. Am. Chem. Soc.*, 2024, **146**, 6638–6651.
15 S. Míguez-Lago, A. L. Llamas-Saiz, M. M. Cid and J. L. Alonso-Gómez, A Covalent Organic Helical Cage with Remarkable Chiroptical Amplification, *Chem. – Eur. J.*, 2015, **21**, 18085–18088.
16 N. Xu, K. Su, E.-S. M. El-Sayed, Z. Ju and D. Yuan, Chiral proline-substituted porous organic cages in asymmetric organocatalysis, *Chem. Sci.*, 2022, **13**, 3582–3588.
17 L. Chen, Z. Chen, W. Wang, C. Chen, Y. Kuboi, C. Zhang, C. Li and S. Zhang, Interwoven Trimeric Cage-Catenanes with Topological Chirality, *J. Am. Chem. Soc.*, 2024, **146**, 30303–30313.
18 Y.-L. Sun, Z. Wang, H. Ma, Q.-P. Zhang, B.-B. Yang, X. Meng, Y. Zhang and C. Zhang, Chiral emissive porous organic cages, *Chem. Commun.*, 2023, **59**, 302–305.
19 Q. Song, J. Yang, K. Zheng, T. Zhang, C. Yuan, L.-M. Yuan and X. Hou, Chiral Memory in Dynamic Transformation from Porous Organic Cages to Covalent Organic Frameworks for Enantiorecognition Analysis, *J. Am. Chem. Soc.*, 2024, **146**, 7594–7604.
20 H. Jędrzejewska and A. Szumna, Making a Right or Left Choice: Chiral Self-Sorting as a Tool for the Formation of Discrete Complex Structures, *Chem. Rev.*, 2017, **117**, 4863–4899.
21 N. Farfán, H. Höpfl, V. Barba, M. E. Ochoa, R. Santillan, E. Gómez and A. Gutiérrez, New perspectives for boronic esters in macrocyclic chemistry, *J. Organomet. Chem.*, 1999, **581**, 70–81.
22 J. Cruz-Huerta, D. Salazar-Mendoza, J. Hernández-Paredes, I. F. Hernández Ahuactzi and H. Höpfl, *N*-containing boronic esters as self-complementary building blocks for the assembly of 2D and 3D molecular networks, *Chem. Commun.*, 2012, **48**, 4241–4243.
23 N. Christinat, R. Scopelliti and K. Severin, Multicomponent assembly of boronic acid based macrocycles and cages, *Angew. Chem., Int. Ed.*, 2008, **47**, 1848–1852.
24 A. D. Herrera-España, H. Höpfl and H. Morales-Rojas, Host-Guest Properties of a Trigonal Iminoboronate Ester Cage Self-Assembled from Hexahydroxytriphenylene, *Eur. J. Org. Chem.*, 2022, e202200383.
25 E. Giraldi, A. B. Depallens, D. Ortiz, F. Fadaei-Tirani, R. Scopelliti and K. Severin, Boronate Ester-Capped Helicates, *Chem. – Eur. J.*, 2020, **26**, 7578–7582.
26 E. Giraldi, R. Scopelliti, F. Fadaei-Tirani and K. Severin, Metal-Stabilized Boronate Ester Cages, *Inorg. Chem.*, 2021, **60**, 10873–10879.
27 G. Zhang, O. Presly, F. White, I. M. Oppel and M. Mastalerz, A permanent mesoporous organic cage with an exceptionally high surface area, *Angew. Chem., Int. Ed.*, 2014, **53**, 1516–1520.
28 G. Zhang, O. Presly, F. White, I. M. Oppel and M. Mastalerz, A shape-persistent quadruply interlocked giant cage catenane with two distinct pores in the solid state, *Angew. Chem., Int. Ed.*, 2014, **53**, 5126–5130.
29 S. M. Elbert, N. I. Regenauer, D. Schindler, W.-S. Zhang, F. Rominger, R. R. Schröder and M. Mastalerz, Shape-Persistent Tetrahedral [4 + 6] Boronic Ester Cages with Different Degrees of Fluoride Substitution, *Chem. – Eur. J.*, 2018, **24**, 11438–11443.
30 M. Hähsler and M. Mastalerz, A Giant [8 + 12] Boronic Ester Cage with 48 Terminal Alkene Units in the Periphery for Postsynthetic Alkene Metathesis, *Chem. – Eur. J.*, 2021, **27**, 233–237.
31 S. Klotzbach and F. Beuerle, Shape-Controlled Synthesis and Self-Sorting of Covalent Organic Cage Compounds, *Angew. Chem., Int. Ed.*, 2015, **54**, 10356–10360.
32 S. Klotzbach, T. Scherpf and F. Beuerle, Dynamic covalent assembly of tribenzotriquinacenes into molecular cubes, *Chem. Commun.*, 2014, **50**, 12454–12457.
33 N. Schäfer, M. Bühler, L. Heyer, M. I. S. Röhr and F. Beuerle, Endohedral Hydrogen Bonding Templates the Formation of a Highly Strained Covalent Organic Cage Compound, *Chem. – Eur. J.*, 2021, **27**, 6077–6085.
34 S. Ivanova, P. Adamski, E. Köster, L. Schramm, R. Fröhlich and F. Beuerle, Size Determination of Organic Cages by

Diffusion NMR Spectroscopy, *Chem. – Eur. J.*, 2024, **30**, e202303318.

35 S. Ivanova, E. Köster, J. J. Holstein, N. Keller, G. H. Clever, T. Bein and F. Beuerle, Isoreticular Crystallization of Highly Porous Cubic Covalent Organic Cage Compounds, *Angew. Chem., Int. Ed.*, 2021, **60**, 17455–17463.

36 P. H. Kirchner, L. Schramm, S. Ivanova, K. Shoyama, F. Würthner and F. Beuerle, A Water-Stable Boronate Ester Cage, *J. Am. Chem. Soc.*, 2024, **146**, 5305–5315.

37 T. P. I. Saragi, T. Spehr, A. Siebert, T. Fuhrmann-Lieker and J. Salbeck, Spiro Compounds for Organic Optoelectronics, *Chem. Rev.*, 2007, **107**, 1011–1065.

38 M. Dobler, M. Dumić, M. Egli and V. Prelog, Chiral Poly (9,9′-spirobifluorene) Crown Ethers, *Angew. Chem., Int. Ed. Engl.*, 1985, **24**, 792–794.

39 V. Alcazar and F. Diederich, Enantioselective Complexation of Chiral Dicarboxylic Acids in Clefts of Functionalized 9,9′-Spirobifluorenes, *Angew. Chem., Int. Ed. Engl.*, 1992, **31**, 1521–1523.

40 G. Das and A. D. Hamilton, Carbohydrate recognition: Enantioselective spirobifluorene diphosphonate receptors, *Tetrahedron Lett.*, 1997, **38**, 3675–3678.

41 A. Lützen, F. Thiemann and S. Meyer, Synthesis of Tetra (BINOL) Substituted Spirobifluorenes, *Synthesis*, 2002, 2771–2777.

42 A. Liesenfeld and A. Lützen, Molecular recognition of isomeric protonated amino acid esters monitored by ESI-mass spectrometry, *Beilstein J. Org. Chem.*, 2014, **10**, 825–831.

43 C. Stobe, I. Pyka, A. Linke, S. Müller, G. Schnakenburg, S. R. Waldvogel and A. Lützen, Synthesis of 9,9′-Spirobifluorenes and 4,5-Diaza-9,9′-spirobifluorenes and Their Application as Affinity Materials for Quartz Crystal Microbalances, *ChemPlusChem*, 2017, **82**, 758–769.

44 T. Piehler and A. Lützen, Enantiomerically Pure *C*2-symmetric Dinuclear Silver(I) and Copper(I) Complexes from a Bis(2,2′-bipyridine)-substituted 9,9′-Spirobifluorene Ligand, *Z. Naturforsch., B: J. Chem. Sci.*, 2010, **65**, 329–336.

45 R. Hovorka, G. Meyer-Eppler, T. Piehler, S. Hytteballe, M. Engeser, F. Topić, K. Rissanen and A. Lützen, Unexpected self-assembly of a Homochiral Metallosupramolecular M4L4 catenane, *Chem. – Eur. J.*, 2014, **20**, 13253–13258.

46 R. Hovorka, S. Hytteballe, T. Piehler, G. Meyer-Eppler, F. Topić, K. Rissanen, M. Engeser and A. Lützen, Self-assembly of metallosupramolecular rhombi from chiral concave 9,9′-spirobifluorene-derived bis(pyridine) ligands, *Beilstein J. Org. Chem.*, 2014, **10**, 432–441.

47 K. Ding, Z. Han and Z. Wang, Spiro skeletons: A Class of Privileged Structure for Chiral Ligand Design, *Chem. – Asian J.*, 2009, **4**, 32–41.

48 Y. Fan, D. W. Kang, S. Labalme and W. Lin, A Spirobifluorene-Based Covalent Organic Framework for Dual Photoredox and Nickel Catalysis, *J. Am. Chem. Soc.*, 2023, **145**, 25074–25079.

49 Y. Liu, C. Wu, Q. Sun, F. Hu, Q. Pan, J. Sun, Y. Jin, Z. Li, W. Zhang and Y. Zhao, Spirobifluorene-Based Three-Dimensional Covalent Organic Frameworks with Rigid Topological Channels as Efficient Heterogeneous Catalyst, *CCS Chem.*, 2021, **3**, 2418–2427.

50 S. Liu, D. Xia and M. Baumgarten, Rigidly Fused Spiro-Conjugated π-Systems, *ChemPlusChem*, 2021, **86**, 36–48.

51 S. Chen and H. Xu, Electroluminescent materials toward near ultraviolet region, *Chem. Soc. Rev.*, 2021, **50**, 8639–8668.

52 S.-Y. Yang, J. Wang, Z. Deng, Y. Xu, X. Su, L. Zhang, S. Yang, R. T. K. Kwok, J. W. Y. Lam and B. Z. Tang, Spiro-materials with aggregation-induced emission, *Matter*, 2024, **7**, 3390–3421.

53 C. Stobe, R. Seto, A. Schneider and A. Lützen, Synthesis, Chiral Resolution, and Absolute Configuration of C2-Symmetric, Chiral 9,9′-Spirobifluorenes, *Eur. J. Org. Chem.*, 2014, 6513–6518.

54 V. Prelog and D. Bedeković, Chirale 2,2′-Polyoxaalkano-9,9′-spirobifluorene, *Helv. Chim. Acta*, 1979, **62**, 2285–2302.

55 F. Thiemann, T. Piehler, D. Haase, W. Saak and A. Lützen, Synthesis of Enantiomerically Pure Dissymmetric 2,2′-Disubstituted 9,9′-Spirobifluorenes, *Eur. J. Org. Chem.*, 2005, 1991–2001.

56 R. G. Clarkson and M. Gomberg, Spirans with Four Aromatic Radicals on the Spiro Carbon Atom, *J. Am. Chem. Soc.*, 1930, **52**, 2881–2891.

57 *Spartan'20*, Wavefunction Inc., Irvine, CA (USA).

58 *The PyMOL Molecular Graphics System, Version 2.5.5*, Schrödinger, LLC.